The Astrophysical Journal Letters, 973:L53 (9pp), 2024 October 1 https://doi.org/10.3847/2041-8213/ad6b29

Redshifted Sodium Transient near Exoplanet Transit

Apurva V. Oza[1,2], Julia V. Seidel[3], H. Jens Hoeijmakers[4], Athira Unni[5,6], Aurora Y. Kesseli[7], Carl A. Schmidt[8], Thirupathi Sivarani[6], Aaron Bello-Arufe[2], Andrea Gebek[9], Moritz Meyer zu Westram[10], Sérgio G. Sousa[11], Rosaly M. C. Lopes[2], Renyu Hu[2,1], Katherine de Kleer[1], Chloe Fisher[12], Sébastien Charnoz[13], Ashley D. Baker[14], Samuel P. Halverson[2], Nick M. Schneider[15], Angelica Psaridi[16], Aurélien Wyttenbach[16], Santiago Torres[17], Ishita Bhatnagar[18], and Robert E. Johnson[19,20]

[1] Division of Geological and Planetary Sciences, California Institute of Technology, Pasadena, USA; oza@caltech.edu
[2] Jet Propulsion Laboratory, California Institute of Technology, Pasadena, USA
[3] European Southern Observatory, Santiago de Chile, Chile
[4] Department of Astronomy and Theoretical Physics, Lund Observatory, Lund, Sweden
[5] Department of Physics and Astronomy, University of California, Irvine, Irvine, CA, USA
[6] Indian Institute of Astrophysics, Bangalore, India
[7] Caltech/IPAC-NASA Exoplanet Science Institute, Pasadena, USA
[8] Center for Space Physics, Boston University, Boston, USA
[9] Sterrenkundig Observatorium, Universiteit Gent, Ghent, Belgium
[10] Physikalisches Institut, Universität Bern, Bern, Switzerland
[11] Instituto de Astrofísica e Ciências do Espaço, Universidade do Porto, CAUP, Porto, Portugal
[12] Department of Physics, University of Oxford, Oxford, UK
[13] Université de Paris, Institut de Physique du Globe de Paris, CNRS, Paris, France
[14] Department of Astronomy, California Institute of Technology, Pasadena, USA
[15] Laboratory for Atmospheric and Space Physics, University of Colorado Boulder, Boulder, CO, USA
[16] Observatoire de Genève, Université de Genève, Genève, Switzerland
[17] Institute of Science and Technology Austria (ISTA), Klosterneuburg, Austria
[18] Birla Institute of Technology and Science, Pilani, India
[19] Department of Physics, New York University, USA
[20] University of Virginia, Charlottesville, USA

Received 2024 June 7; revised 2024 July 18; accepted 2024 August 2; published 2024 September 30

Abstract

Neutral sodium (Na I) is an alkali metal with a favorable absorption cross section such that tenuous gases are easily illuminated at select transiting exoplanet systems. We examine both the time-averaged and time-series alkali spectral flux individually, over 4 nights at a hot Saturn system on a ∼2.8 day orbit about a Sun-like star WASP-49 A. Very Large Telescope/ESPRESSO observations are analyzed, providing new constraints. We recover the previously confirmed residual sodium flux uniquely when averaged, whereas night-to-night Na I varies by more than an order of magnitude. On HARPS/3.6 m Epoch II, we report a Doppler redshift at $v_{\Gamma,\mathrm{NaD}} = +9.7 \pm 1.6\,\mathrm{km\,s^{-1}}$ with respect to the planet's rest frame. Upon examining the lightcurves, we confirm night-to-night variability, on the order of ∼1%–4% in NaD, rarely coinciding with exoplanet transit, not readily explained by stellar activity, starspots, tellurics, or the interstellar medium. Coincident with the $\sim+10\,\mathrm{km\,s^{-1}}$ Doppler redshift, we detect a transient sodium absorption event $dF_{\mathrm{NaD}}/F_\star = 3.6\% \pm 1\%$ at a relative difference of $\Delta F_{\mathrm{NaD}}(t) \sim 4.4\% \pm 1\%$, lasting $\Delta t_{\mathrm{NaD}} \gtrsim 40$ minutes. Since exoplanetary alkali signatures are blueshifted due to the natural vector of radiation pressure, estimated here at roughly $\sim-5.7\,\mathrm{km\,s^{-1}}$, the radial velocity is rather at $+15.4\,\mathrm{km\,s^{-1}}$, far larger than any known exoplanet system. Given that the redshift magnitude v_Γ is in between the Roche limit and dynamically stable satellite orbits, the transient sodium may be a putative indication of a natural satellite orbiting WASP-49 A b.

Unified Astronomy Thesaurus concepts: Natural satellites (Extrasolar) (483); Exoplanet astronomy (486); Transmission spectroscopy (2133); Radial velocity (1332); Doppler shift (401)

1. Introduction

Sodium and potassium are alkali metals, observed in the vapor form, which are remarkably strong absorbers in transmission spectroscopy (Seager & Sasselov 2000). Neutral sodium gas (Na I) at a transiting exoplanet system, for instance, may be probed at tenuous densities with line-of-sight columns far below $N \ll 10^{12}\,\mathrm{Na\,cm^{-2}}$ (Draine 2011), roughly 0.01 picobars or ∼4 nanopascals for an isothermal atmosphere on an Earth-sized planet. The favorable cross section of Na I enabled its first detection at the hot Saturn HD209458b (Charbonneau et al. 2002) in low-resolution by Hubble Space Telescope. New high-resolution precision by Very Large Telescope (VLT)/ESPRESSO since identified previously interpreted planetary sodium as stellar from HD209458 (Casasayas-Barris et al. 2021). It was suggested shortly after the initial exoplanetary detections that since neutral sodium is photoionized within minutes (Huebner & Mukherjee 2015) on a few-day orbit, compared to the ∼few hours transit duration of transiting exoplanets (Johnson et al. 2006), alkali metals may be exogenic. In other words, since sodium is uniquely probed as a neutral, a continuous supply of exogenic neutral atoms may be preferred, especially at high altitudes above the planet's surface, where Na I is probed.

Since sodium and potassium are D-line resonance doublets, the D_2/D_1 ratio also allows for spectral characterization

(Gebek & Oza 2020), which so far has helped constrain a range of possible sodium densities systematically at up to ten exoplanet systems where neutral sodium has been reliably identified (Langeveld et al. 2022). Here we examine one of the dozens of known alkali exoplanet systems (or transiting planetary systems with reported alkali detections) WASP-49b, reported to host a high-altitude layer of neutral sodium at roughly $\sim$1.5 R_p, thought to be thermal and nonisothermal (Cubillos et al. 2017; Wyttenbach et al. 2017; Fisher & Heng 2019; Oza et al. 2019; Gebek & Oza 2020). Large-aperture, low-resolution observations similar to the successful James Webb Space Telescope (JWST) also allow for coarse analyses to assess the presence of alkalies. We note, for instance, observations with the VLT/FORS2 (Lendl et al. 2016) and recently, the Gran Telescopia Canarias/OSIRIS (Jiang et al. 2023) do not detect previously identified Na I or K I, motivating the need for several more transit observations and in-depth high-resolution analyses.

WASP-49 A (2MASS 06042146-1657550) is a faint ($m_G = 11.29 \pm 0.1$) Sun-like star discovered by the Wide Angle Search for Planets (WASP; Pollacco et al. 2006) now known to be in a binary star system common to most transiting exoplanets (Mugrauer 2019). Subsequently in 2012, its transiting Saturn-mass companion WASP-49 A b was discovered (Lendl et al. 2012) and characterized by VLT/FORS2 (Lendl et al. 2016). The hot Saturn exoplanet system transits its Sun-like star every 2.78 days or 66.7 hr for a duration of $2.15^{+0.02}_{-0.01}$ hr or $\sim$128 minutes. This transit timescale with a precision of roughly 1 minute and overexposure time of $\sim$10 minutes defines our temporal uncertainties to describe neutral sodium, as we will describe below. Here, we seek to probe the Hill sphere of WASP-49 A b in NaD light with 3 nights of HARPS/ESO 3.6 m data and new VLT/ESPRESSO 8.2 m data. The Hill sphere is the gravitational sphere of influence where natural satellites are expected to be stable for $\sim$Gyr within $\sim\frac{1}{2}$ Hill sphere, as estimated by several dynamical works (Domingos et al. 2006; Cassidy et al. 2009; Kisare & Fabrycky 2024). This is below an altitude of $\sim$2.0 R_p for WASP-49 A b and above the Roche limit for a rocky body at $\sim$1.2 R_p (Oza et al. 2019). Na I at the Jupiter system is ultimately sourced by volcanic NaCl from its satellite Io (Küppers & Schneider 2000) sputtering into a "banana cloud" of order $\sim R_J$ (Haff et al. 1981; Schneider & Brown 1981). A fast component largely escapes Jupiter $\gtrsim$100 km s^{-1}, forming a $\sim$1000 R_J sodium cloud (Mendillo et al. 1990). Jupiter's gravitationally bound component $\lesssim$60 km s^{-1} is fueled by two plasma processes: (1) "jet" localized to Io from dissociative recombination of $NaCl^+$ formed via charge exchange with photoionized gas in Io's ionosphere (Schmidt et al. 2023) and (2) "stream" extending beyond $\gtrsim$10 R_J neutralized by ions Na^+ or NaX^+ entrained in the diffuse Io plasma torus far from Io (Wilson et al. 2002). Our high-resolution approach, led by the initial detection at HD189733b (Redfield et al. 2008) is able to identify Doppler-shifted alkali absorption, in time. Since Doppler shifts in Jovian Na I spectra pinpoint the radial velocity of Io and its ion chemistry (Cremonese et al. 1992), we are, in principle, able to indirectly trace natural satellites. New star–planet system parameters probed by our new high-resolution VLT/ESPRESSO observations are reported in Table 1, while Table 2 indicates the start of each exoplanet transit epoch. Based on our new large-aperture observations of the star, we constrain a smaller stellar mass at $M_\star = 0.894 \pm 0.04\, M_\odot$ and a slightly smaller planet mass $M_p = 0.365 \pm 0.019\ M_J$ than previous studies (Lendl et al. 2012; Stassun et al. 2017; Wyttenbach et al. 2017). We first present our transmission spectra observations in Section 2; upon analysis, we confirm neutral sodium at the resonance line doublet in Section 3 (time-averaged) and Section 4 (sodium lightcurves). Finally, we discuss possible interpretations in Section 5.

2. Neutral Alkali Metal Observations

We present 4 nights of time-resolved high-resolution data for WASP-49 A near exoplanet transit. The first three epochs of observations began on UT 2015 December 6, 2015 December 31, and 2016 January 14 using HARPS/ESO 3.6 m (Mayor et al. 2003; Lovis et al. 2006) and on 2020 December 16 using VLT/ESPRESSO (Pepe et al. 2021). In Section 3, we present time-averaged transmission spectra results centered at the sodium D resonance lines (Na D at $\lambda_{D_2} = 5889.950$ and $\lambda_{D_1} = 5895.924$ Å), and in Section 4, we construct lightcurves of neutral sodium.

Our ESPRESSO/VLT 8.2 m observations provide a first large-aperture epoch compared to three HARPS/3.6 m epochs monitoring the exoplanet Hill sphere (see Table 2). A second ESPRESSO/VLT epoch was disturbed by strong winds during planetary ingress; however, the in-transit and egress data remain useful in evaluating the stellar continuum and activity, as well as measuring fundamental star–planet properties (Table 1), such as the system metallicity $\chi_{Fe/H}$ following Sousa et al. (2008). We use only one VLT/ESPRESSO epoch for the transmission spectrum. In the first VLT/ESPRESSO transit (2020 December 15), the first four exposures with shorter exposure times (300 s instead of 360 s) had approximately 50% lower flux and were discarded for consistency. Additionally, three epochs of HARPS data, previously analyzed by Wyttenbach et al. (2017), were reanalyzed, similar to the ESPRESSO data. The signal-to-noise ratio (SNR) range, SNR56, is provided for the 56th échelle order near the NaD doublet at 5889.95 and 5895.92 Å. To correct for telluric features around the sodium doublet, we employed `molecfit`, version 1.5.1 (Kausch et al. 2015; Smette et al. 2015), demonstrated to remove Earth's water vapor lines near the sodium doublet in several works, e.g., HD189733b (Allart et al. 2017), WASP-76b (Seidel et al. 2019), WASP-121b (Hoeijmakers et al. 2020), WASP-166 (Seidel et al. 2020a), WASP-127, (Seidel et al. 2020b), HAT-P-57b, KELT-7b, KELT-17b, KELT-21b, MASCARA-1b, and WASP-189b (Stangret et al. 2022). We combined all spectra in the observer's rest frame and verified that the telluric lines were corrected down to the noise level of the combined spectrum. No telluric sodium emission or Moon contamination was detected in fiber B (on-sky observations). Moreover, we carefully inspected Earth's (telluric) rest-frame velocities (Table 1, v_{bary}) for Na I and did not detect any, ruling out sodium at Earth's barycenter. The data were analyzed following the procedure at WASP-76b (Seidel et al. 2019) in the NaD wavelength range. Significant scatter was observed due to flux differences at the planetary sodium position relative to stellar sodium lines. Stellar sodium absorption reduces the SNR if planetary sodium overlaps with the same wavelength range. ESPRESSO exposures during transit had shorter exposure times (360 s compared to 600 s for HARPS), causing flux to be dominated by red noise at the center of stellar sodium line cores. The average spectral flux was 1500, while the flux in the stellar line core was 30–120, a decrease by 1–2 orders of magnitude. Similar studies masked

Table 1
Star–Planet System Parameters

Parameter	Variable	Value	References
Stellar Parameters			
Name	WASP-49 A	⋯	...
Gaia DR3 ID	GDR3ID	2991284369063612928	(1)
Apparent Magnitude	m_G (Gaia) (mag)	11.29 ± 0.10	(1)
Spectral Type	i	G6V	...
Stellar Age	$t_\star$ (Gyr)	7 ± 2 Gyr	(2)
Stellar Photosphere Temperature	$T_{\rm eff}$ (K)	5543 ± 61	(2)
Stellar Gravity (spec)	$\log g$ (cm s^{-2})	4.37 ± 0.10	(2)
Stellar Gravity (Gaia)	$\log g$ (cm s^{-2})	4.38 ± 0.03	(2)
Stellar Metallicity	[Fe/H] (dex)	-0.08 ± 0.04	(2)
Stellar Micro Velocity	$v_{\rm mic}$ (km s^{-1})	0.79 ± 0.02	(2)
Stellar Macro Velocity	$v_{\rm mac}$ (km s^{-1})	2.91 ± 0.09	(2)
Stellar Radial Velocity	$v\sin i$ (km s^{-1})	1.93 ± 0.25	(2)
Stellar Mass	$M_\star$ ($M_\odot$)	$0.894^{+0.039}_{-0.035}$	(2)
Stellar Radius	$R_\star$ ($R_\odot$)	0.976 ± 0.034	(3)
Stellar Density	$\rho_\star$ (g cm^{-3})	1.43 ± 0.19	(4)
Stellar Rotational Velocity	$v_{\star,\rm rot}$ (K_1)	57.5 ± 2.1 m s^{-1}	(5)
Planet Parameters			
Exoplanet Transit Midpoint	T_0 (BJD)	$2457377.596934 \pm 0.000080$	(6)
Planet/Star Ratio	$R_p/R_\star$	0.116 ± 0.0007	(6)
Impact Parameter	b	$0.7704^{+0.0072}_{-0.0077}$	(5)
Planet Transit Duration	t_{14} (hr)	$2.146^{+0.022}_{-0.007}$	(2)
Planet Mass	M_p (M_J]	0.365 ± 0.019	(2)
Planet Radius	R_p (R_J)	1.115 ± 0.047	(7)
Planet Orbital Period	τ_P (days)	$2.78173691 \pm 0.00000014$	(6)
Planet Density	ρ_p (g cm^{-3})	0.288 ± 0.006	(5)
Radiative Equilibrium Temperature	$T_{\rm p,eq}$ (K)	1400	...
Velocity Parameters			
Planet Orbit (RV semiamplitude)	K_p (km s^{-1})	151.6	...
System (star+planet) RV	v_γ (km s^{-1})	41.7261 ± 0.0011	...
Barycentric Velocity	$v_{\rm bary,I}$ (km s^{-1})	$6.20 \rightarrow 6.92$	...
	$v_{\rm bary,II}$ (km s^{-1})	$-3.87 \rightarrow -3.07$	...
	$v_{\rm bary,III}$ (km s^{-1})	$-9.3 \rightarrow -8.6$	...
	$v_{\rm bary,IV}$ (km s^{-1})	$2.65 \rightarrow 3.05$	...

Notes. RV designates radial velocity. Barycentric velocity corrections are provided as ranges for each individual epoch (I → IV) in kilometers per second.
References. (1) Gaia Collaboration et al. 2023; (2) this work; (3) Lendl et al. 2012; (4) Stassun et al. 2017; (5) Wyttenbach et al. 2017; (6) Kokori et al. 2023; (7) Bonomo et al. 2017.

Table 2
High-resolution Observations

EPOCH	UT Date	Instrument	#Spectra[a]	$\Delta\ t_{\rm exp}$ (minutes)	SNR56	Air Mass[b]	Seeing
I	2015-12-06	HARPS[c]	41(14/27)	10	21–33	1.9−1.0−1.3	not recorded
II	2015-12-31	HARPS[c]	42(12/30)[d]	10	10–38	1.4−1.0−2.2	0.5–1.3
III	2016-01-14	HARPS[c]	40(13/27)	10	22–40	1.2−1.0−2.3	0.5−1.0
IV	2020-12-16	ESPRESSO[e]	62(36/26)	6	21–26	1.60–1.15−1.00	0.6
V	2021-02-18[f]	ESPRESSO[e]	17(12/5)	8.3	32–27	1.15–1.65	0.5–1.0

Notes.
[a] # Spectra parentheses show the total (in-/out-of-) transit spectra after processing exposures. SNR56 range and and ^b airmass at the beginning, center, and
[b] air Mass at the beginning, center, and end of each transit.
[c] ESO program ID 096.C-0331; PI: Ehrenreich.
[d] Two out-of-transit exposures were rejected due to emission features either stemming from cosmic rays or the instrument.
[e] ESO Program ID Prog.ID = 106.21QX.001, 106.21QX.003; PI:Oza.
[f] Partial transit + egress. Planetary ingress was not observed due to wind, rendering the baseline too short for meaningful analysis. The duration of each epoch is indicated in hours.

the trace of the stellar sodium line (Barnes et al. 2016; Borsa & Zannoni 2018; Seidel et al. 2020a, 2020b); we also masked a window of 4 km s^{-1} in the stellar rest frame across all four epochs for consistency. The Rossiter–Mclaughlin (RM) effect, generally a concern when evaluating Na I (Casasayas-Barris et al. 2020), describes the additional shift in wavelength for transmission spectra due to the rotation of the star as the planet crosses the stellar surface. Wyttenbach et al. (2017) investigated various instrumental, telluric, and stellar influences on the transmission spectrum and used the reloaded RM method (Cegla et al. 2016) to estimate < 100 ppm or $\lesssim$0.01% of an RM effect, concluding either a pole-on transit or indeed an extremely slow-rotating host star, with $v\sin i_\star \lesssim 0.46$ km s^{-1}. Therefore, the RM effect did not have a measurable impact on the HARPS transmission spectrum as it was below the noise level for ESPRESSO data. Upon reduction, we reproduced the time-averaged transmission spectra and detection levels from both Wyttenbach et al. (2017) and Langeveld et al. (2022). Notably, time-averaged alkali depths may vary based on flux-averaged bin widths, a factor carefully examined by Langeveld et al. (2022) for ten alkali exoplanet systems, alongside variable D_2/D_1 alkali ratios from optically thick (Seager & Sasselov 2000) to optically thin systems (Gebek & Oza 2020). We note that while our time-averaged signature over the three epochs (Section 3) agrees largely with Wyttenbach et al. (2017) and Langeveld et al. (2022), our time-resolved signature does not (Section 4). This is likely due to our choice of not discarding exposures we believe were significant SNRs when examining their propagated error in the lightcurves (Section 4).

The high-resolution WASP-49 A b spectrum *averaged* over three epochs is shown in several independent works (Cubillos et al. 2017; Wyttenbach et al. 2017; Fisher & Heng 2019; Oza et al. 2019; Langeveld et al. 2022); however, here we seek to examine each night *individually*. We separate our analysis technique across two components centered at the sodium doublet: Section 3.2 NaD spectra (time-averaged sodium) and Section 4 NaD lightcurves (instantaneous sodium).

3. Time-averaged Sodium

We build four transmission spectra following Allart et al. (2020) and Seidel et al. (2023b, 2023a). Here, we focus on alkali line profiles and their apparent variability. We perform a Bayesian retrieval framework using a No U-Turn Sampler (Betancourt 2017) implemented with `Jax`and `NumPyro` (Bradbury et al. 2018; Bingham et al. 2019; Phan et al. 2019). To model the doublet, we assume that both lines are Gaussian with centroid velocity v_0 and width σ, with a flat continuum at c, and the dimensionless parameter β is used to scale the uncertainties, indicating that the errors have been marginally overestimated. Overall, we see distinct Na I variability in the sodium flux absorption amplitudes from epoch to epoch: $d\mathcal{F}_{\rm Na}/\mathcal{F}_\star$ (Epoch I) $= -0.8\% \pm 0.3\%$, $d\mathcal{F}_{\rm Na}/\mathcal{F}_\star$ (Epoch II) $= -3.8\% \pm 0.8\%$, $d\mathcal{F}_{\rm Na}/\mathcal{F}_\star$ (Epoch III) $= +0.4\% \pm 0.5\%$, and$d\mathcal{F}_{\rm Na}/\mathcal{F}_\star$ (Epoch IV) $= -0.8\% \pm 0.2\%$. Best-fit models are shown in Figure 1 along with posterior distributions in Figure 2, and accompanying values tabulated in Table 3. The sodium flux on HARPS Epoch 2 on 2015 December 31, detected at roughly 5σ, appears to be the primary source of the time-averaged sodium flux (Wyttenbach et al. 2017; Langeveld et al. 2022). HARPS Epoch 3 on 2016 January 14 is consistent with a null hypothesis (zero flux absorption at the sodium doublet) with a $p_{dF(\lambda)}$-value $= 0.22$. On the other hand, HARPS Epoch I and II, and ESPRESSO Epoch IV have a nontrivial $p_{dF(\lambda)}$-value $= 10^{-2.4}$, $10^{-5.9}$, and $10^{-4.5}$, respectively. Based on the average D_2 line absorption, we compute the minimum neutral line-of-sight sodium column density based on the identified flux absorption at Na D_2 line center (Draine 2011): $N_{\rm Na,1}(\lambda) \sim 10^{10.5\pm0.4}$ cm^{-2}, $N_{\rm Na,2}(\lambda) = 10^{11.2\pm0.7}$ cm^{-2}, $N_{\rm Na,3}(\lambda) < 10^{10.2\pm0.1}$ cm^{-2}, and $N_{\rm Na,4}(\lambda) \sim 10^{10.5\pm0.4}$ cm^{-2}. Order-of-magnitude sodium variability is not expected for stable planetary atmospheres. Given that Epoch 3 was at a higher SNR, it is surprising that HARPS did not identify a time-averaged flux signature based on the column density of $N_{\rm Na,3}$. Since the distinct epoch-to-epoch variability is not well known for exoplanets, we investigate several hypotheses that may contribute an alternative sodium signature along our line of sight. Furthermore, as demonstrated by Langeveld et al. (2022), measurable differences in line depths from independent reductions (Wyttenbach et al. 2017) can occur due to binning, which further motivates time-dependent investigations. A bandpass of 0.75 Å was used in the current analysis, whereas Wyttenbach et al. (2017) used 0.4 Å. Choices on discarding certain exposures may lead to the current indication of emission in Night 3. However, as we will see in Section 4, examining the data in time is likely more useful for validating independent exposures.

3.1. Spurious Stellar Sodium Signals

Care is taken during our analysis to consider stellar NaD absorption, stellar lightcurve NaD absorption, and interstellar medium (ISM) absorption. The 11th magnitude Sun-like star system WASP-49 A (G6V) is not identified as an active star unlike brighter transiting alkali exoplanet systems, e.g., HD189733 (K-type star). Photometry from TESS and EulerCam show no significant flares, especially in NaD. Furthermore, unlike the brighter alkali exoplanet system HD209458b, WASP-49 A b is minimally affected by the RM effect (Casasayas-Barris et al. 2018; Langeveld et al. 2022) with a trivial $v\sin i$ $\sim 0.9 \pm 0.3$ km s^{-1}. Other systems such as WASP-189b (Prinoth et al. 2023) with larger $v\sin i$ $\sim 93.1 \pm 1.7$ km s^{-1} (Lendl et al. 2020) and HAT-P-70 b (Bello-Arufe et al. 2023) at $v\sin i$ $\sim 99.87 \pm 0.65$ km s^{-1} (Zhou et al. 2019) also exhibit alkali sodium local to the planetary systems. Regarding ISM sodium features, Langeveld et al. (2022) reported significant and narrow ISM sodium absorption for several exoplanets, including WASP-21 and WASP-189, with intensities of $\gtrsim$90%. A Na I survey along 1005 lines of sight within 300 pc was extensively studied by Lallement et al. (2003) and Welsh et al. (2010). Of course, if the residual sodium absorption is indeed due to ISM, the signature would be identical for all transits, which is not the case; see Section 4. Indeed, no such features were seen for WASP-49 A (Langeveld et al. 2022). Misaligned with the expected radial velocity (RV) of the ISM relative to Earth's barycenter, a secondary sodium peak is Doppler blue-shifted from the stellar rest frame at ~ -19.5 km s^{-1}, matching the feature reported by Wyttenbach et al. (2017) at roughly -20 km s^{-1}. Unlike ISM-contaminated stars, this feature is weaker at only $\sim$10%. Several more nights of long-baseline, large-aperture, échelle observations at the sodium doublet are needed to characterize the variability of this sodium feature, potentially linked to the identified Doppler shifts.

A stellar spot can be ruled out based on time-dependent stellar spectra from HARPS/3.6 m, VLT/ESPRESSO (2021 October 11), and UVES (2016 January 7) observations. The

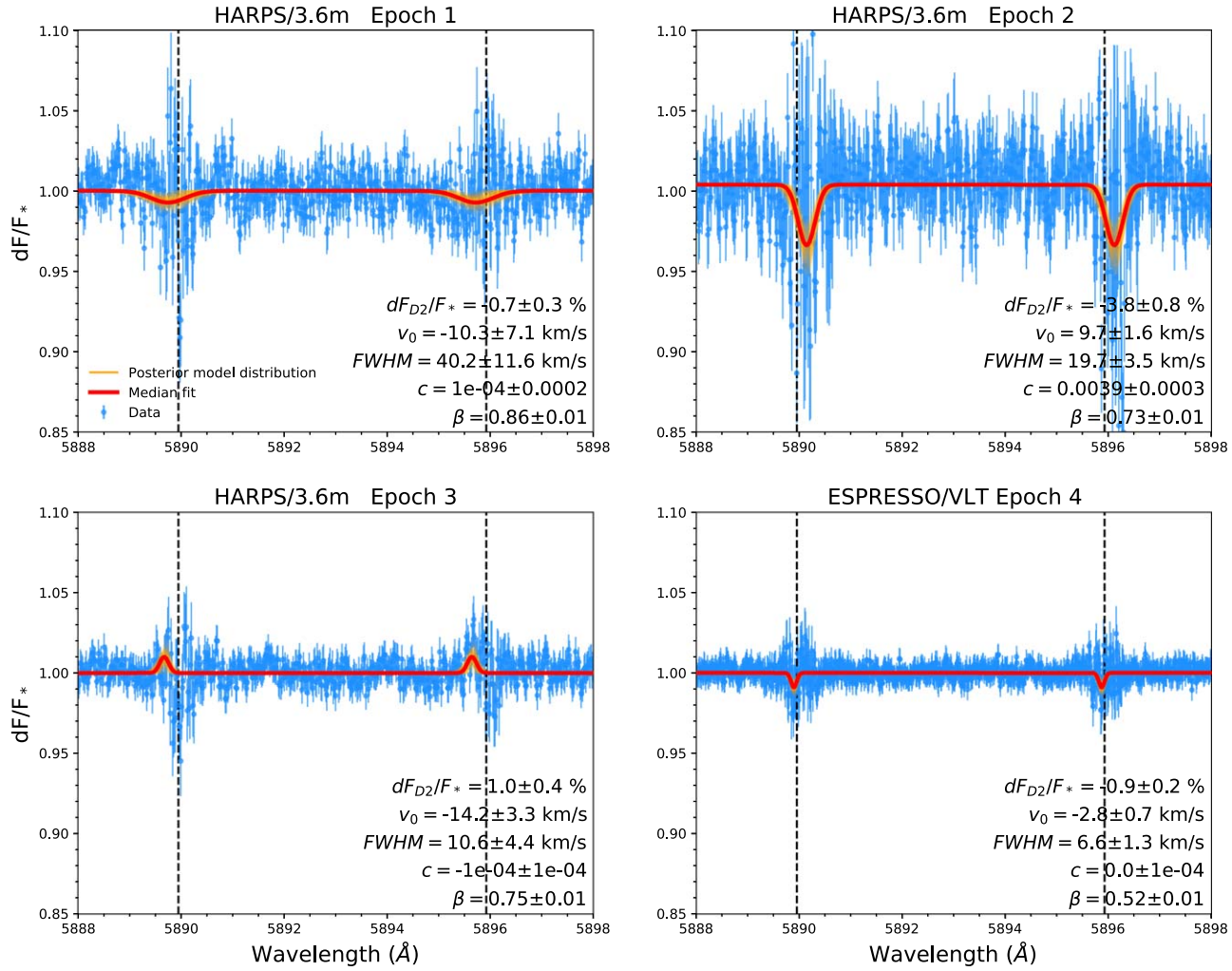

Figure 1. Transmission spectrum of neutral atomic sodium (Na I) over four epochs, with raw data (blue), posterior model (orange), and median fit (red). (a) Epoch I: 2015 December 6; (b) Epoch II: 2015 December 31; (c) Epoch III: 2016 January 14; (d) Epoch IV: 2020 December 15 (ESPRESSO/VLT). The Epoch II *net* Doppler shift is measured to be a redshift $v_0 = +9.7 \pm 1.6\,\mathrm{km\,s^{-1}}$. Epoch III is a nondetection. In Epoch I, a blueshift is seen, at low significance. Companion residual lightcurves for each epoch are provided (Figure 3).

stellar sodium remains identical in each frame and wavelength, making a spurious event or stellar spot crossing unlikely. Control experiments by Wyttenbach et al. (2017) using Mg I (5183.604 Å) and Ca I lines (6122.217 Å, 6162.173 Å) also rule out stellar chromospheric activity. WASP-49 A hosts a binary companion $\sim 0.34\,M_\odot$, separated by $\sim$443 au from recent Gaia analyses (Mugrauer 2019). Far more observations are necessary to understand binary star dynamics' implications; however, fiber-fed spectroscopy does indeed resolve WASP-49 A. Telluric sodium contamination is not detected in our spectral reduction at Earth's reference frame. In Section 3.2 we look deeper into the astrophysical origin of the neutral sodium signature by examining radial velocity signatures.

3.2. Doppler Redshift of Neutral Sodium

We investigate the significance of Doppler shifts that appear to be present in some of the nights to learn more about the residual sodium signatures. Figure 2 in particular indicates a Doppler shift in Epoch 2. At a larger significance than Epoch 2's $\sim 5\sigma$ flux absorption (Section 3), the significance of the radial velocity detection in Epoch 2 is larger at $\sim 6\sigma$. The sodium doublet is significantly redshifted in Epoch 2, at a radial velocity of $+9.7 \pm 1.6\,\mathrm{km\,s^{-1}}$. This is surprising as substantial alkali redshifts have not been measured at exoplanet systems, as most neutral atoms would be preferentially blueshifted $\sim -5\,\mathrm{km\,s^{-1}}$ for H_2O at HD189733b (Brogi et al. 2016; Boucher et al. 2021; Blain et al. 2024) and Na I (Redfield et al. 2008). HD189733b also exhibits variable Doppler shift signatures in Na I (Louden & Wheatley 2015) from $v_\Gamma = -5.3^{+1.0}_{-1.4} \rightarrow +2.3^{+1.3}_{-1.5}\,\mathrm{km\,s^{-1}}$. In fact, high-resolution time-series data of Io's sodium in eclipse (Schmidt et al. 2023) is a solar system demonstration that substantial Doppler *redshifts* of an alkali metal at a transiting system are uniquely fueled by natural satellites. Io fuels Jupiter's sodium exosphere out to a radius of $\sim 500\,R_\mathrm{p}$ (Mendillo et al. 1990). Mercury's planetary sodium tail, which extends to $\sim 1000\,R_\mathrm{p}$ (Schmidt et al. 2010), is again, only observed to be Doppler blueshifted and not redshifted due to radiation pressure. At the distance of WASP-49 A b, accounting for radiation pressure, the net system velocity of the residual sodium is at $+15.4 \pm 1.6\,\mathrm{km\,s^{-1}}$. This sodium velocity corresponds to a synchronous orbit at an altitude of $\sim 2.44\,R_\mathrm{p}$ at roughly $\sim$19 hr. If astrophysical, the null hypothesis for Epoch 2's Doppler shift (p_Γ-value $= 10^{-9.2}$) yields a less-than-a-billion chance for the Doppler redshift of optically thick Na I to be spurious. Similarly, if we force the

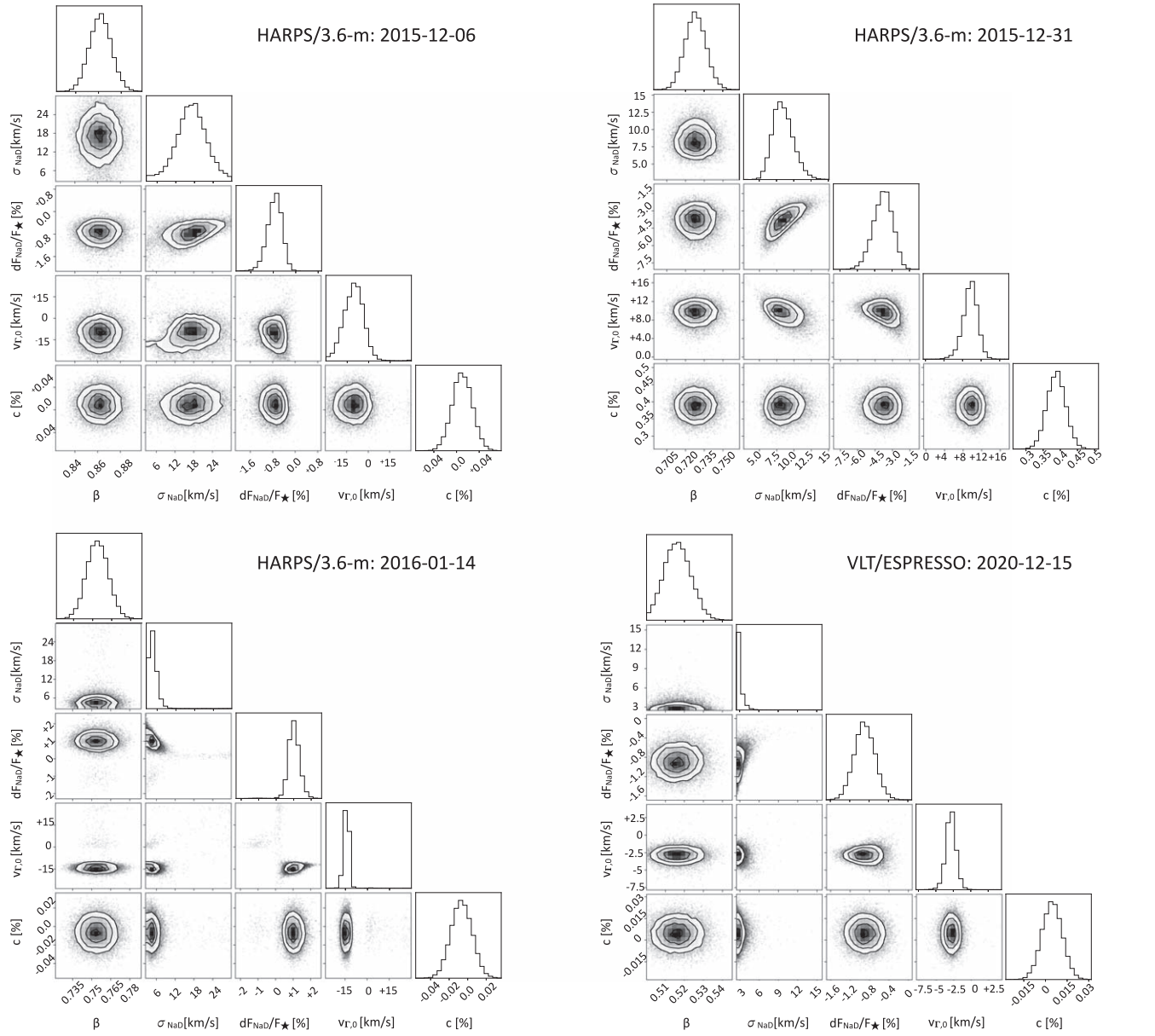

Figure 2. Four-panel Gaussian fit runs for a nominal sodium absorption solution where $f_{D_2/D_1} = 1.0$. (a) Epoch I: 2015 December 6; (b) Epoch II: 2015 December 31; (c) Epoch III: 2016 January 14; (d) Epoch IV: 2020 December 15. Posterior distributions of the model parameters describe the Na doublet as a pair of Gaussians with the same amplitude $dF_{\rm Na}/F_{\star}$, centroid velocity shift v_0, width σ, and continuum c. The uncertainties are scaled with β, which is a free fitting parameter.

Table 3
Posterior Values from Figure 1 Are Tabulated Here with 1σ Gaussian Uncertainties

Parameter	Epoch I	Epoch II	Epoch III	Epoch IV
$dF_{\rm Na,\lambda}/F_{\star}$ (%)	-0.736 ± 0.263	-3.768 ± 0.833	1.006 ± 0.355	-0.896 ± 0.212
v_0 (km s^{-1})	-10.28 ± 7.1	$+9.72 \pm 1.6$	-14.18 ± 3.26	-2.84 ± 0.75
c (ppm)	99.78 ± 176.35	3886.68 ± 271.43	-67.28 ± 112.73	45.97 ± 69.44
β	0.86 ± 0.01	0.73 ± 0.01	0.75 ± 0.01	0.52 ± 0.01
σ_V (km s^{-1})	17.09 ± 4.92	8.35 ± 1.5	4.52 ± 1.88	2.79 ± 0.56
T_K	145729 ± 12077	34788 ± 1123 K	10193 ± 1763 K	3884 ± 156.4 K

Note. $dF_{\rm Na,\lambda}/F_{\star}$ (%) is the absorption flux at sodium D-line center, v_0 is the Doppler shift from the exoplanet's rest frame, c is the continuum offset in parts per million, β is a normalization parameter, σ_V is the FWHM of the line width, and T_K is the kinetic temperature (derived from σ_V and $v_{\rm Th}$).

Gaussian spectral fit to $D_2/D_1 > 1$ (in the optically thin regime), we still detect a significant Doppler redshift up to $+12$ km s^{-1}, with a preferred value near $+6$ km s^{-1}, although we do not believe this solution is physical. For further credence regarding a redshifted radial velocity component, and more certainty regarding unknown systematics affecting the sodium absorption signature, we construct relative sodium lightcurves below in Section 4. This is in supplement to previous analyses

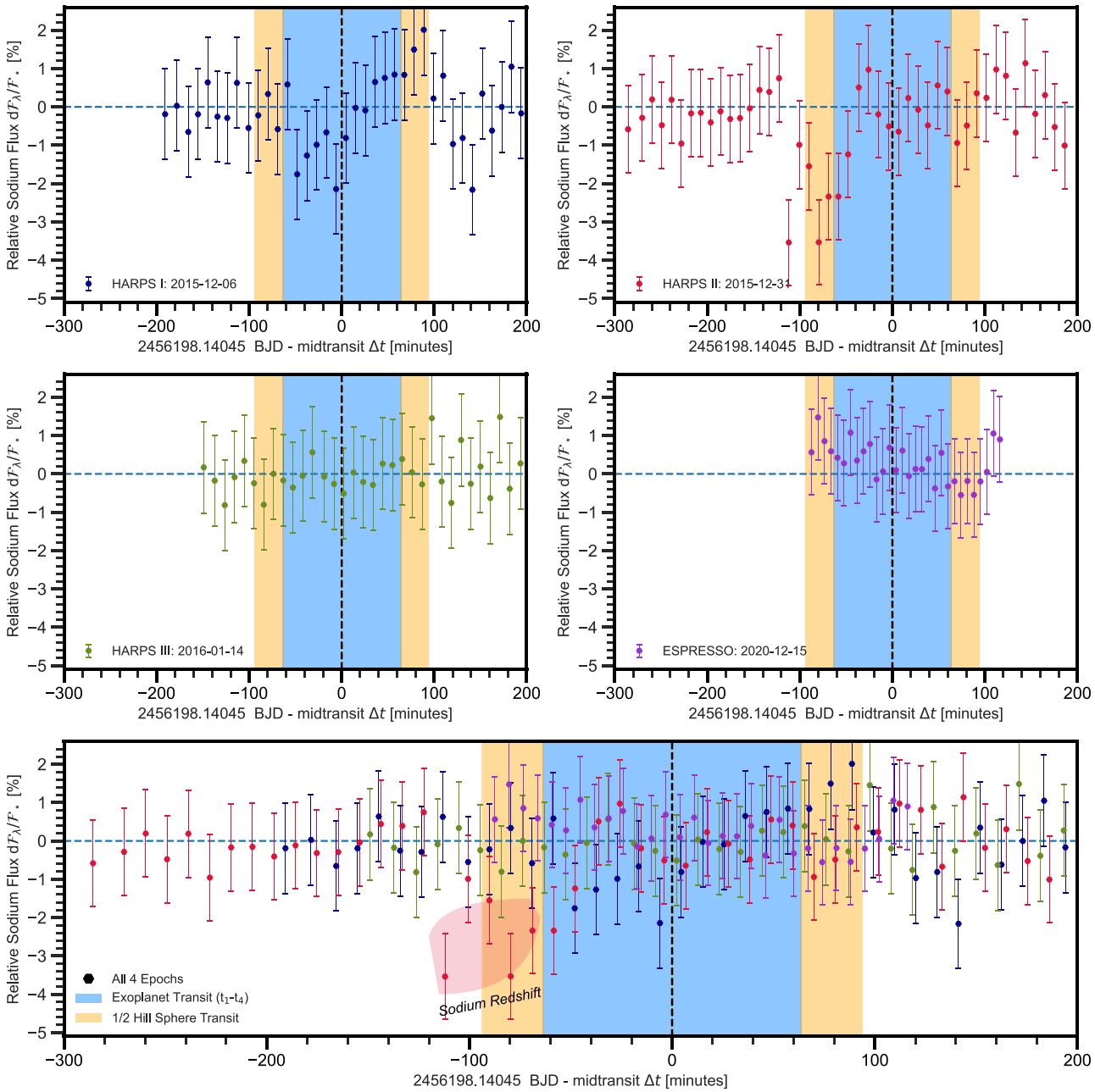

Figure 3. HARPS/ESPRESSO neutral sodium residual lightcurves ($d\lambda = 0.75$ Å). Black data points are Na D_2 spectra at four epochs centered at the transit of the hot Saturn WASP-49 A b, $t_{0,\mathrm{exoplanet}}$. Yellow bands mark one-half of the Hill sphere transit time, and blue bands mark the $t_1 - t_4$ exoplanet transit time.

of residual sodium at this system, which did not time resolve the Na D_2 line (Wyttenbach et al. 2017; Langeveld et al. 2022). By examining the time evolution of sodium, we are able to pinpoint when in time (exposure times of 5–10 minutes) the observed redshift occurred relative to the exoplanet's transit across the stellar surface.

4. Sodium Light Curves

By separating the four observations in time, we are able to examine the evolution of the sodium gas and directly probe *when* the Doppler-shifted sodium appears in terms of the known exoplanet midcenter time t_0. The ephemeris, accurate to subminute precision (Kokori et al. 2023), then provides tight constraints on when the exoplanet surface and its Hill sphere begin to transit. In this way, residual lightcurves may rule out symmetric atmospheric or magnetospheric geometries in time. Relative lightcurves for four individual transits of WASP-49b are extracted *in time* at 1σ standard deviation in Figure 3, where the SNR is indicated in Table 2. The lightcurves are extracted by averaging the relative absorption signal of the Na D_2 and D_1 lines (over two bands with bandwidth $\Delta\lambda = 0.75$ Å) and normalizing the transit depth to continuum bands without absorption lines (Wyttenbach et al. 2017).

To not bias the feature seen in the second HARPS transit, HARPS relative absorption lightcurves were generated with a master-out spectrum only taking into account spectra taken far away from ingress and egress excluding each time $\delta = 0.015$ in phase before and after the transit to exclude a sodium

absorption source linked to the planet's trajectory present in our master-out spectrum.

The four panels show that the relative sodium absorption signal is highly variable and transient, changing between epochs, as well as within the individual transits for the first 2 nights, and is not at all associated with the planetary transit window of ∼129 minutes, unlike other alkaline exoplanets. For instance, sodium at WASP-76b (also taken with HARPS/3.6 m) and WASP-172b (VLT/ESPRESSO) steadily absorbs at $\lesssim$0.5% relative to the much brighter star at higher SNR and is more or less within the exoplanet transit window over 3 individual nights on HARPS (Seidel et al. 2019) and 2 nights of ESPRESSO (Seidel et al. 2023b).

In stark contrast, our current candidate WASP-49 A b does not have consistent absorption near t_0 in each transit. In fact, the sodium lightcurve is nearly flat in certain epochs.

The vanishing 2%–4% signal in epochs three and four is difficult to reconcile with absorption from a stable planetary atmosphere or magnetosphere (Lai et al. 2010; Czesla et al. 2022). The minimum change in the sodium column from Epoch 2 to Epoch 3 is × 9.5. For Epoch 2, we examine the SNR at 5500 Å to evaluate potential false positives. The 6σ Doppler redshift occurs close to ∼03:20 UT, long before exoplanet ingress at 05:22 UT near the sodium event, where we do identify a decreased SNR. Weather conditions in ESO Astronomical Site Monitor archives find no clouds detected on the pyrgeometer ("clear"), sufficient wind speed (∼4 m s^{-1}), and stable temperatures (∼15°C) and humidity below 30%. We conclude that while the transit depth of the feature may be marginally overestimated, it is not an artifact due to atmospheric conditions (e.g., clouds). One possible hypothesis for an increase in seeing is a larger jet stream velocity along our line of sight, which is known to affect seeing (Vernin 1986) and degrade SNR.

Moreover, in Epoch 2 the signal peaks midway through the ingress of ∼one-half the Hill sphere (orange bands in Figure 3), long *before* first contact of the planet (blue bands indicate first t_1 and fourth t_4 contact of the planet in Figure 3). The first event occurs for a duration of 10 minutes, and the second event of sodium for another $\Delta t \sim 40$ minutes, coincident with the exoplanet's Hill sphere and Roche limit transit time. The feature is shaded in red in Figure 3. When examining the radial velocity residuals at the sodium doublet in Epoch 2, we indeed find that the large Doppler redshift is coincident with the $\gtrsim$40 minute, sodium feature occurring in the Hill sphere, over a minimum precision on the order of the exposure time ∼10 minutes.

5. Conclusion

We report significant kinematic and flux variability of neutral sodium absorption that does not coincide with the known exoplanet transit time of the hot Saturn WASP-49 A b. The transient sodium detection on the night of UT 2015 December 31 (exoplanet transit midpoint at UT 2016 January 1 05:22) persists for over ≈40 minutes at a relative 4.4σ significance *in temporal*, 4.8σ *in spectral*, and 6.0σ in RV space. While the 2015 December 6 feature is less significant at a relative flux of 2.7σ, it too diminishes over ≈40 minutes prior to transit mid-center. The significances for other nights are low, primarily due to the dimness of the distant star at an apparent magnitude $m_v = 11.35$.

Searches for companion ions and neutrals (e.g., S, O, Mg, and Si) in optical and IR are encouraged to test the electrodynamics of rapidly ionized sodium (Koskinen et al. 2014). The presence of neutral potassium at the K I doublet at 7664.90 Å and 7698.96 Å was searched for with ESPRESSO, however, not detected, as expected, as it is far more tenuous than its companion alkali signature (Na I) in Epoch 4. The Keck Planet Finder, as well as future high-resolution instruments on the Thirty Meter Telescope, the Giant Magellan Telescope, or the Extremely Large Telescope, will help us pinpoint the origin of the transient metal signatures reported here.

If a variable sodium source exists within the planetary system, we cannot be sure of its orbit nor its cloud geometry based on five transits alone. More transits are needed and would be especially efficient since a single transit duration endures ∼2.14 hr + 1 hr of ingress and egress, and it monitors the entirety of the planetary Roche limit (Roche 1873) and the $\sim\frac{1}{2}$ Hill sphere gravitational boundary discussed in Section 1. If satellite orbits endure only ∼6–11 hr, our observations probe up to ∼28%–55% of putative orbits per observation. A viable explanation may be that a satellite's sodium is uniquely illuminated at particular phases, for instance at maximum insolation during occultation or planetary shadow during eclipse. Circumstellar disk observations have revealed evaporating bodies too small to otherwise be seen, by exogenic Na I at LkHα 234 (Chakraborty et al. 2004), β Pictoris (Hobbs et al. 1985; Beust et al. 1990, 2024), and possibly 55 Cancri-e (Ridden-Harper et al. 2016; Meier Valdés et al. 2023). NaD absorption due to putative natural satellites and their accompanying clouds/tori have been suggested only by time-averaged spectra at several exoplanet systems thus far (Oza et al. 2019; Gebek & Oza 2020; Hoeijmakers et al. 2020; Schmidt 2022; Meyer zu Westram et al. 2024), however here we present an initial time-resolved signature. Both time-averaged and time-resolved cases encourage significant observational follow-up and study of tidal resonances, some of which is underway (Barr et al. 2023; Tokadjian & Piro 2023). The gas variability is similar to ultraviolet, visible, or infrared observations of alkali, molecular oxygen, and water lines seen at Jupiter's satellites (Brown & Hill 1996; Thomas 1996; Retherford et al. 2007; Thomas 2022; de Kleer et al. 2023).

Acknowledgments

The research described in this Letter was carried out in part at the Jet Propulsion Laboratory, California Institute of Technology, under a contract with the National Aeronautics Space Administration, © 2024. California Institute of Technology. Government sponsorship acknowledged. A.V.O. and J.V.S. thank M. Lendl for constraints and discussions on the mass of WASP-49 A b. S.G.S acknowledges the support from FCT through Investigador FCT contract nr. CEECIND/00826/2018 and POPH/FSE (EC).

Data Availability

ESO data is available publicly on ESO's science archive facility at archive.eso.org/eso/eso_archive_main.html.

ORCID iDs

Apurva V. Oza https://orcid.org/0000-0002-1655-0715
Julia V. Seidel https://orcid.org/0000-0002-7990-9596
H. Jens Hoeijmakers https://orcid.org/0000-0001-8981-6759
Athira Unni https://orcid.org/0000-0001-6093-5455

Aurora Y. Kesseli https://orcid.org/0000-0002-3239-5989
Carl A. Schmidt https://orcid.org/0000-0002-6917-3458
Thirupathi Sivarani https://orcid.org/0000-0003-0891-8994
Aaron Bello-Arufe https://orcid.org/0000-0003-3355-1223
Andrea Gebek https://orcid.org/0000-0002-0206-8231
Moritz Meyer zu Westram https://orcid.org/0000-0003-0446-688X
Sérgio G. Sousa https://orcid.org/0000-0001-9047-2965
Rosaly M. C. Lopes https://orcid.org/0000-0002-7928-3167
Renyu Hu https://orcid.org/0000-0003-2215-8485
Katherine de Kleer https://orcid.org/0000-0002-9068-3428
Chloe Fisher https://orcid.org/0000-0003-0652-2902
Sébastien Charnoz https://orcid.org/0000-0002-7442-491X
Ashley D. Baker https://orcid.org/0000-0002-6525-7013
Samuel P. Halverson https://orcid.org/0000-0003-1312-9391
Nick M. Schneider https://orcid.org/0000-0001-6720-5519
Angelica Psaridi https://orcid.org/0000-0002-4797-2419
Aurélien Wyttenbach https://orcid.org/0000-0001-9003-7699
Santiago Torres https://orcid.org/0000-0002-3150-8988
Robert E. Johnson https://orcid.org/0000-0001-7798-5918

References

Allart, R., Lovis, C., Pino, L., et al. 2017, A&A, 606, A144
Allart, R., Pino, L., Lovis, C., et al. 2020, A&A, 644, A155
Barnes, J. R., Haswell, C. A., Staab, D., & Anglada-Escudé, G. 2016, MNRAS, 462, 1012
Barr, A. C., Brasser, R., Dobos, V., & Quick, L. C. 2023, in Io: A New View of Jupiter's Moon, Astrophysics and Space Science Library, ed. R. M. C. Lopes, K. de Kleer, & J. T. Keane (New York: Springer), 323
Bello-Arufe, A., Knutson, H. A., Mendonça, J. M., et al. 2023, AJ, 166, 69
Betancourt, M. 2017, arXiv:1701.02434
Beust, H., Lagrange-Henri, A. M., Vidal-Madjar, A., & Ferlet, R. 1990, A&A, 236, 202
Beust, H., Milli, J., Morbidelli, A., et al. 2024, A&A, 683, A89
Bingham, E., Chen, J. P., Jankowiak, M., et al. 2019, J. Mach. Learn. Res., 20, 1
Blain, D., Sánchez-López, A., & Mollière, P. 2024, AJ, 167, 179
Bonomo, A. S., Desidera, S., Benatti, S., et al. 2017, A&A, 602, A107
Borsa, F., & Zannoni, A. 2018, A&A, 617, A134
Boucher, A., Darveau-Bernier, A., Pelletier, S., et al. 2021, AJ, 162, 233
Bradbury, J., Frostig, R., Hawkins, P., et al. 2018, JAX: composable transformations of Python+NumPy programs, v0.2.5, GitHub, http://github.com/google/jax
Brogi, M., de Kok, R. J., Albrecht, S., et al. 2016, ApJ, 817, 106
Brown, M. E., & Hill, R. E. 1996, Natur, 380, 229
Casasayas-Barris, N., Palle, E., Stangret, M., et al. 2021, A&A, 647, A26
Casasayas-Barris, N., Pallé, E., Yan, F., et al. 2018, A&A, 616, A151
Casasayas-Barris, N., Pallé, E., Yan, F., et al. 2020, A&A, 635, A206
Cassidy, T. A., Mendez, R., Arras, P., Johnson, R. E., & Skrutskie, M. F. 2009, ApJ, 704, 1341
Cegla, H. M., Lovis, C., Bourrier, V., et al. 2016, A&A, 588, A127
Chakraborty, A., Ge, J., & Mahadevan, S. 2004, ApJL, 606, L69
Charbonneau, D., Brown, T. M., Noyes, R. W., & Gilliland, R. L. 2002, ApJ, 568, 377
Cremonese, G., Thomas, N., Barbieri, C., & Pernechele, C. 1992, A&A, 256, 286
Cubillos, P. E., Fossati, L., Erkaev, N. V., et al. 2017, ApJ, 849, 145
Czesla, S., Lampón, M., Sanz-Forcada, J., et al. 2022, A&A, 657, A6
de Kleer, K., Milby, Z., Schmidt, C., Camarca, M., & Brown, M. E. 2023, PSJ, 4, 37
Domingos, R. C., Winter, O. C., & Yokoyama, T. 2006, MNRAS, 373, 1227
Draine, B. T. 2011, Physics of the Interstellar and Intergalactic Medium (Princeton, NJ: Princeton Univ. Press)
Fisher, C., & Heng, K. 2019, ApJ, 881, 25
Gaia Collaboration, Vallenari, A., Brown, A. G. A., et al. 2023, A&A, 674, A1
Gebek, A., & Oza, A. V. 2020, MNRAS, 497, 5271
Haff, P. K., Watson, C. C., & Yung, Y. L. 1981, JGR, 86, 6933
Hobbs, L. M., Vidal-Madjar, A., Ferlet, R., Albert, C. E., & Gry, C. 1985, ApJL, 293, L29
Hoeijmakers, H. J., Seidel, J. V., Pino, L., et al. 2020, A&A, 641, A123
Huebner, W. F., & Mukherjee, J. 2015, P&SS, 106, 11
Jiang, C., Chen, G., Pallé, E., et al. 2023, A&A, 675, A62
Johnson, R. E., Smith, H. T., Tucker, O. J., et al. 2006, ApJL, 644, L137
Kausch, W., Noll, S., Smette, A., et al. 2015, A&A, 576, A78
Kisare, A., & Fabrycky, D. 2024, MNRAS, 527, 4371
Kokori, A., Tsiaras, A., Edwards, B., et al. 2023, ApJS, 265, 4
Koskinen, T. T., Yelle, R. V., Lavvas, P., & Cho, J. Y-K. 2014, ApJ, 796, 16
Küppers, M., & Schneider, N. M. 2000, GeoRL, 27, 513
Lai, D., Helling, C., & van den Heuvel, E. P. J. 2010, ApJ, 721, 923
Lallement, R., Welsh, B. Y., Vergely, J. L., Crifo, F., & Sfeir, D. 2003, A&A, 411, 447
Langeveld, A. B., Madhusudhan, N., & Cabot, S. H. C. 2022, MNRAS, 514, 5192
Lendl, M., Anderson, D. R., Collier-Cameron, A., et al. 2012, A&A, 544, A72
Lendl, M., Csizmadia, S., Deline, A., et al. 2020, A&A, 643, A94
Lendl, M., Delrez, L., Gillon, M., et al. 2016, A&A, 587, A67
Louden, T., & Wheatley, P. J. 2015, ApJL, 814, L24
Lovis, C., Pepe, F., Bouchy, F., et al. 2006, Proc. SPIE, 6269, 62690P
Mayor, M., Pepe, F., Queloz, D., et al. 2003, Msngr, 114, 20
Meier Valdés, E. A., Morris, B. M., Demory, B. O., et al. 2023, A&A, 677, A112
Mendillo, M., Baumgardner, J., Flynn, B., & Hughes, W. J. 1990, Natur, 348, 312
Meyer zu Westram, M., Oza, A. V., & Galli, A. 2024, JGRE, 129, e2023JE007935
Mugrauer, M. 2019, MNRAS, 490, 5088
Oza, A. V., Johnson, R. E., Lellouch, E., et al. 2019, ApJ, 885, 168
Pepe, F., Cristiani, S., Rebolo, R., et al. 2021, A&A, 645, A96
Phan, D., Pradhan, N., & Jankowiak, M. 2019, arXiv:1912.11554
Pollacco, D. L., Skillen, I., Collier Cameron, A., et al. 2006, PASP, 118, 1407
Prinoth, B., Hoeijmakers, H. J., Pelletier, S., et al. 2023, A&A, 678, A182
Redfield, S., Endl, M., Cochran, W. D., & Koesterke, L. 2008, ApJL, 673, L87
Retherford, K. D., Spencer, J. R., Stern, S. A., et al. 2007, Sci, 318, 237
Ridden-Harper, A. R., Snellen, I. A. G., Keller, C. U., et al. 2016, A&A, 593, A129
Roche, E. 1873, Essai Sur la Constitution et l'origine du Système Solaire (Paris: Gauthier Villars), 1873
Schmidt, C., Sharov, M., de Kleer, K., et al. 2023, PSJ, 4, 36
Schmidt, C. A. 2022, FrASS, 9, 801873
Schmidt, C. A., Wilson, J. K., Baumgardner, J., & Mendillo, M. 2010, Icar, 207, 9
Schneider, N. M., & Brown, R. A. 1981, BAAS, 13, 730
Seager, S., & Sasselov, D. D. 2000, ApJ, 537, 916
Seidel, J. V., Borsa, F., Pino, L., et al. 2023a, A&A, 673, A125
Seidel, J. V., Ehrenreich, D., Bourrier, V., et al. 2020a, A&A, 641, L7
Seidel, J. V., Ehrenreich, D., Wyttenbach, A., et al. 2019, A&A, 623, A166
Seidel, J. V., Lendl, M., Bourrier, V., et al. 2020b, A&A, 643, A45
Seidel, J. V., Prinoth, B., Knudstrup, E., et al. 2023b, A&A, 678, A150
Smette, A., Sana, H., Noll, S., et al. 2015, A&A, 576, A77
Sousa, S. G., Santos, N. C., Mayor, M., et al. 2008, A&A, 487, 373
Stangret, M., Casasayas-Barris, N., Pallé, E., et al. 2022, A&A, 662, A101
Stassun, K. G., Collins, K. A., & Gaudi, B. S. 2017, AJ, 153, 136
Thomas, N. 1996, A&A, 313, 306
Thomas, N. 2022, ExA, 54, 791
Tokadjian, A., & Piro, A. L. 2023, AJ, 165, 173
Vernin, J. 1986, Proc. SPIE, 628, 142
Welsh, B. Y., Lallement, R., Vergely, J. L., & Raimond, S. 2010, A&A, 510, A54
Wilson, J. K., Mendillo, M., Baumgardner, J., et al. 2002, Icar, 157, 476
Wyttenbach, A., Lovis, C., Ehrenreich, D., et al. 2017, A&A, 602, A36
Zhou, G., Huang, C. X., Bakos, G. Á, et al. 2019, AJ, 158, 141